TECHNOLOGY

Continuous-flow, electrically-triggered, single cell-level electroporation

Mingde Zheng[1], Joseph J. Sherba[1], Jerry W. Shan[2], Hao Lin[2], David I. Shreiber[1] & Jeffrey D. Zahn[1]

Electroporation creates transient openings in the cell membrane, allowing for intracellular delivery of diagnostic and therapeutic substances. The degree of cell membrane permeability during electroporation plays a key role in regulating the size of the delivery payload as well as the overall cell viability. A microfluidic platform offers the ability to electroporate single cells with impedance detection of membrane permeabilization in a high-throughput, continuous-flow manner. We have developed a flow-based electroporation microdevice that automatically detects, electroporates, and monitors individual cells for changes in permeability and delivery. We are able to achieve the advantages of electrical monitoring of cell permeabilization, heretofore only achieved with trapped or static cells, while processing the cells in a continuous-flow environment. We demonstrate the analysis of membrane permeabilization on individual cells before and after electroporation in a continuous-flow environment, which dramatically increases throughput. We have confirmed cell membrane permeabilization by electrically measuring the changes in cell impedance from electroporation and by optically measuring the intracellular delivery of a fluorescent probe after systematically varying the electric field strength and duration and correlating the pulse parameters to cell viability. We find a dramatic change in cell impedance and propidium iodide (PI) uptake at a pulse strength threshold of 0.87 kV/cm applied for a duration of 1 ms or longer. The overall cell viability was found to vary in a dose dependent manner with lower viability observed with increasing electric field strength and pulse duration. Cell viability was greater than 83% for all cases except for the most aggressive pulse condition (1 kV/cm for 5 ms), where the viability dropped to 67.1%. These studies can assist in determining critical permeabilization and molecular delivery parameters while preserving viability.

***Keywords*: Single Cell; Electroporation; Permeabilization; Microfluidics; and Molecular-Transport.**

INNOVATION

This work demonstrates the impedance detection of cell membrane permeabilization in a continuous-flow environment at high sensitivity. The operation of an automated, single cell-level electroporation microchip was successfully demonstrated through both electrical and optical monitoring of cell permeabilization across a wide range of pulse applications. Our results show that a large number of cells can be individually treated, and their viability can be correlated with the applied pulse parameters. This microchip has the potential to bridge the gap between single cell analyses via immobilization and high-throughput cell-electroporation devices, drastically improving cell viability for different cell types without empirically derived electroporation protocols.

INTRODUCTION

The controlled introduction of foreign vectors and molecules into living cells has been a major focus in biomedical research and clinical medicine[1–3]. Intracellular delivery of biomolecules (e.g. nucleic acids and proteins) and therapeutics agents (e.g. siRNA-loaded nanoparticles)[4,5] enables the study of basic cell functions and the transformation of cell phenotype and potentially genotype and enhances the understanding and screening for disease states. Non-viral approaches to cell transfection remain popular because of potential drawbacks associated with viral-mediated delivery, including immunogenicity, cytotoxicity, limited space on a virus package, and possible mutagenesis/tumorigenesis[6,7]. Among non-viral methods, electroporation is a widely used, effective, and high-throughput technique that is relatively low cost, easy to operate, safe, fast, and efficient in transfecting many cell types[7,8]. With the application of an electric pulse of appropriate strength and duration, transient, aqueous pores are induced through the cell membrane, permitting access and molecular delivery to the intracellular space. However, obtaining efficient delivery without compromising cell viability requires the development of optimized electroporation protocols for each individual cell type and potentially each payload. These protocols are efficient for cell types with a large-enough cell sample to accommodate lower delivery efficiency or viability, but for cell types having a limited cell number and/or an inhomogeneous cell population (i.e. non-immortalized or primary cells), protocol development becomes difficult. To address these concerns, we have previously quantitatively modeled and evaluated the molecular-transport phase of electroporation to rationally design electroporation protocols that are safer and more effective[9–16]. However, differences in the sensitivity of different cell types to electroporation remains a challenge.

[1] Department of Biomedical Engineering, Rutgers, The State University of New Jersey, Piscataway, NJ 08854, USA. [2] Department of Mechanical and Aerospace Engineering, Rutgers, The State University of New Jersey, Piscataway, NJ 08854, USA. Correspondence should be addressed to J.D.Z. (jdzahn@soe.rutgers.edu).

Received 3 November 2016; accepted 9 January 2017; published online 15 February 2017; doi:10.1142/S2339547817500017

Therefore, by utilizing the advancements made in microfabrication techniques, we have sought to create a micro-electroporation platform that can electroporate flowing cells on an individual-cell basis to provide an automated, reliable, and controllable approach for permeabilizing the cell membrane, allowing for efficient intracellular transport of biomolecules while maximally preserving cell viability.

Single cell electroporation is typically performed in one of two regimes: static cell or continuous-flow. Static cell electroporation requires the immobilization of the targeted cell at a prescribed location, permitting repeated comprehensive monitoring of changes in the electrical characteristics of the same cell. Among the first groups to demonstrate single cell electroporation, Ryttsén *et al.* mechanically positioned a cell between two electrodes with a micropipette[17]. The work by Rubinsky and colleagues later demonstrated the use of a three-layer microchannel to immobilize single cells via suction, within an opening between two conducting electrode plates. They carried out electroporation and measured electrical current indicative of cell membrane permeabilization[18]. In 2004, Khine *et al.* reported the development of a 2-dimensional microchannel to trap and electroporate individual cells. In addition to the detection of a cell membrane-permeabilization threshold, they also reported evidence of cell membrane resealing[19,20]. More recently, there has been an increasing interest in developing methods that electrically monitors the electroporation events. An example is the microdevice developed by Guo and Zhu, which dielectrophoretically traps single cells prior to electroporation and measurement[21]. Another example is the microdevice developed by Bürgel *et al.* that "shuttles" a cell back and forth between an electroporating and an impedance sensing electrode[22]. These studies provide the foundation for conducting electroporation measurements at the single cell-level. However, one significant drawback of immobilized cell studies is the inherent low throughput of the devices, which limits analysis to only a few cells at a time.

To improve throughput, a separate research direction has focused on the electroporation of cells in a continuous-flow environment. This approach is realized by flowing cells across a pair of electrodes within an electroporation zone, where a prescribed electric field is applied to permeabilize the traversing cells. Lu *et al.* implemented a saw-tooth electrode design parallel to the cell flow field, which resulted in highly focused electric fields at the saw-tooth tips, allowing the electrical lysis of the passing cells[23]. Using a simpler design, Wang and Lu demonstrated the ability to amplify the electric field strength by manipulating microchannel geometry. When an electric field is applied across a geometric constriction, the field strength increases, electroporating cells as they flow through the constriction. This allowed the study of cell swelling and rupture[24]. Another recent approach used a combination of large flow tubes with a small electrode needle array. Zhao *et al.* showed that by creating large channel space for cells to flow through, throughput of electroporation can be greatly enhanced; and by integrating a well-organized electroporating needle array in the flow tubes, uniform electric field and low voltage applied to the passing cells produces efficient transfection[25]. Although these devices electroporate cells in a high throughput manner, little is known about the individual cell state during the electroporation process. Analysis is typically through live-dead staining following cell collection or by tracking the delivery of a vector or molecular dye. Additionally, such devices often rely on empirically-obtained protocols specific to an individual cell type.

In this report, we aim to combine these approaches to take advantage of the precision single cell electrical measurements demonstrated through immobilized cell studies while electropermeabilizing a large number of cells in a continuous-flow environment. We have designed a microfluidic device that operates automatically to detect the entrance of an individual cell into an electroporation zone with a high signal-to-noise ratio (SNR), and subsequently applies a user-defined electroporation pulse to the cell in transit. Cell membrane impedance is continuously monitored, and both optical and electrical measurements are conducted before and immediately after pulse application. By performing a parametric study of different pulse strengths, measuring the percentage change in cell impedance in real-time, and assessing cell viability after collection, we demonstrate the device's ability to measure and alter cell membrane permeabilization in a continuous-flow fashion, and enable intracellular transport of small molecules.

RESULTS AND DISCUSSIONS

Operation principle and modeling

The operation of the automatic-electroporation system starts with the perfusion of single cells through a microfluidic-channel constriction (250 (L) μm × 25 (W) μm × 10 (D) μm), an active region consisting of both sensing and electroporation electrodes (300 μm inter-electrode spacing), hereafter referred to as the electroporation zone (**Fig. 1a**). The electroporation zone was designed as a microchannel constriction-based geometry[24]. It provides three distinctive advantages: (1) a large current-displacement signal for single cell detection; (2) a high cell-volume fraction which increases the impedance change SNR during permeabilization; and (3) geometric amplification of the electroporation pulse to lower the input voltage requirement, thus avoiding unwanted effects such as Joule heating, and electrolysis. COMSOL simulation (COMSOL Multiphysics 4.2a, COMSOL) of the microchannel in **Fig. 1b** shows the amplification of the electric field as a function of channel length. When an electric potential of 12 volts is applied to the electrodes, a 0.45 kV/cm electric field is measured at the constriction. The presence of a cell within the constriction further increases the local resistance, amplifying the electric field to 0.7 kV/cm around the cell.

When the electroporation process is initiated, the sensor continuously monitors each cell's passage across the electroporation zone. Cell entry into the electroporation zone produces a sharp current drop in comparison to the buffer baseline due to the high impedance of the cell, which also serves as the basis for the well-known resistive-pulse sensing technique[26–28]. Once a cell has been identified, a solid state switch is actuated to automatically apply an electroporation pulse with a predefined electric field strength and duration via a customized signal processing program in LabVIEW (LabVIEW Professional Edition 2015, National Instruments) (**Fig. 1c**). Immediately following the pulse application, the current is again monitored to record any post-pulse impedance changes from the cell prior to its departure from the electroporation zone.

To determine the optimal channel geometry and sensing frequency required to detect cell membrane permeabilization, a cell/electrolyte equivalent circuit was constructed to model the single-cell electrical-impedance response in a microfabricated flow cytometer. This circuit model was adapted from previous models[26,29] to account for the dramatic increase in cell membrane conductance during electroporation. The model allows determination of the impedance of a cell suspended in buffer between a pair of electrodes as shown in **Fig. 1d**. V_{in} is the excitation voltage input, C_{DL} is the double layer capacitance, C_{mem} is the capacitance of the cell membrane and R_i is the cell's internal resistance. R_m and C_m are the resistance and capacitance of the extracellular media, respectively. To reflect the overall impedance change as a result of cell membrane permeabilization by electroporation, a variable R_{mem} was implemented in parallel to C_{mem}. Lastly, G represents a pre-amplifier that converts current into voltage for digital processing. Comparing the resultant impedance magnitude $|Z|$ for a suspended cell before and after electroporation allowed us to determine the optimal frequency range in which to expect the largest change in impedance magnitude, $\Delta|Z|$. By varying extracellular buffer conductivity and cell volume fraction, we found that a frequency range between 1 and 10 kHz provided the greatest sensitivity, i.e., largest $\Delta|Z|$, for the experimental conditions (**Supplementary Fig. 1**), which included a buffer conductivity of 100 μS/cm at a 5% cell volume fraction (**Supplementary Fig. 2**). The formula and values for calculating the overall impedance change are reported in **Supplementary Information S1**.

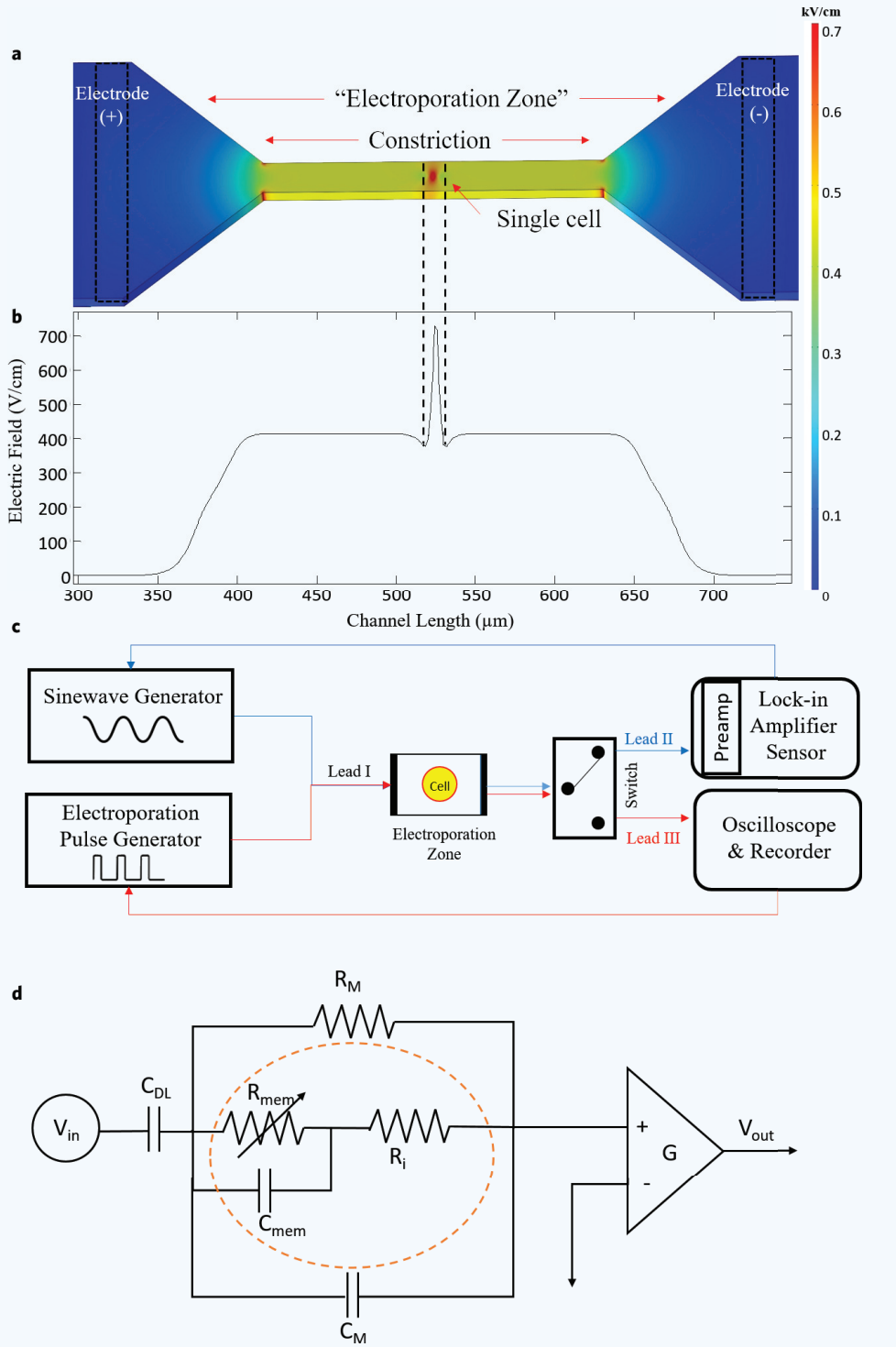

Figure 1 (**a**) COMSOL simulation of the electric field distribution in the electroporation zone with the inclusion of a cell. (**b**) Centerline trace of the electric field magnitude along the channel length. Note an amplification factor of 1.75 × the nominally applied field. (**c**) Schematic illustrating the sensory and electroporation setup of the system. (**d**) Electrical circuit representation of a suspended cell under detection.

Automated cell detection and electroporation

Automated detection of single cells and immediate pulse application to each cell with a throughput of 1.3 cells/sec is demonstrated in **Fig. 2**. The magnitude of the electrical current drop due to the cell's presence in the electroporation zone remains constant. An estimated cell-transit time of 250 ms provided an ample temporal window for electroporation and post-pulse impedance measurement. In this representative plot, the vertical red line depicts the application of a prescribed electroporation pulse, in this case a 1.05 kV/cm electric field for 5.0 ms. A sharp rise in current is immediately observed after administering the pulse. This jump in current results from the increase in cell membrane conductance and is characteristic of the formation of pores as a result of electroporation-induced cell membrane permeabilization. This phenomena has previously been reported by other researchers using microfluidic-based patch-clamping methods[18,19]. As the cell departs from the channel constriction, the electrical signal returns to the buffer-solution baseline. This process repeats for each cell traversing through the electroporation zone. A SNR of 37 dB was measured for the single cell detection. The system maintained a 97% accuracy in detecting and pulsing each cell as compared to optical observations. Error was primarily attributed to the occasional tailgating of multiple cells, leading to multiple-pulse application to each cell in transit and an unreliable impedance measurement. In these experiments, a lower density cell suspension was used to decrease the likelihood of multiple cells entering the electroporation zone at the same time but this also decreased the cell throughput to 1.3 cells/s.

Cell membrane permeabilization analysis

By varying the strength and duration of the electroporation pulse, we demonstrate changes in the cell impedance that are characteristic of the degree of cell membrane permeabilization. As shown in **Fig. 3**, the measured cell current responses for five representative cells are superimposed at the time of pulse application. When the electric field was kept constant at 1.05 kV/cm while altering the pulse durations from 0 to 5.0 ms, a longer pulse duration creates a greater jump in current between the electrodes, indicating a higher degree of membrane permeabilization. A full characterization of the cell membrane response as a function of both electric field strength and duration is shown in **Fig. 4**. To account for cell-to-cell variations due to size differences, the change in the permeabilization current from the cell baseline (ΔI_p) was first

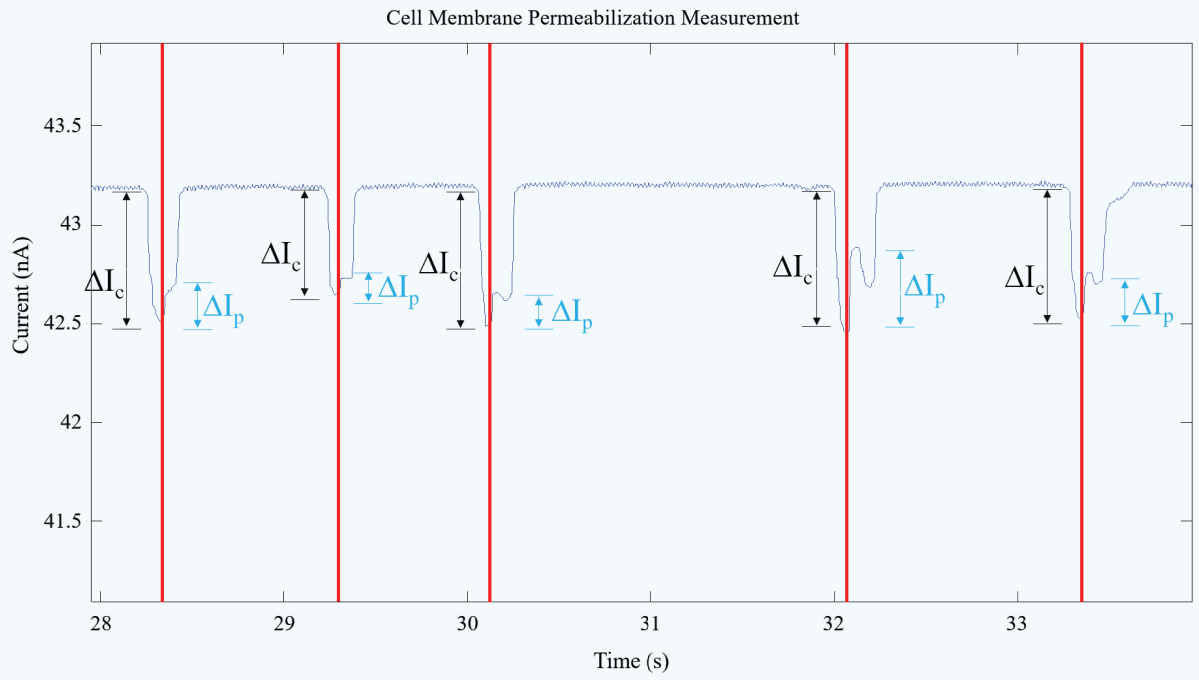

Figure 2 Resistive pulse-based detection of flowing single cells across the channel constriction. Current displacement of each cell entering the pulsing zone is measured as ΔI_c from the baseline current. The red lines indicate the administration of an electroporation pulse. The current "jump" following the pulse is measured as ΔI_p. A flow rate of 0.1 µL/min was used to obtain a sufficient cell transit window for observing post-pulse cell responses.

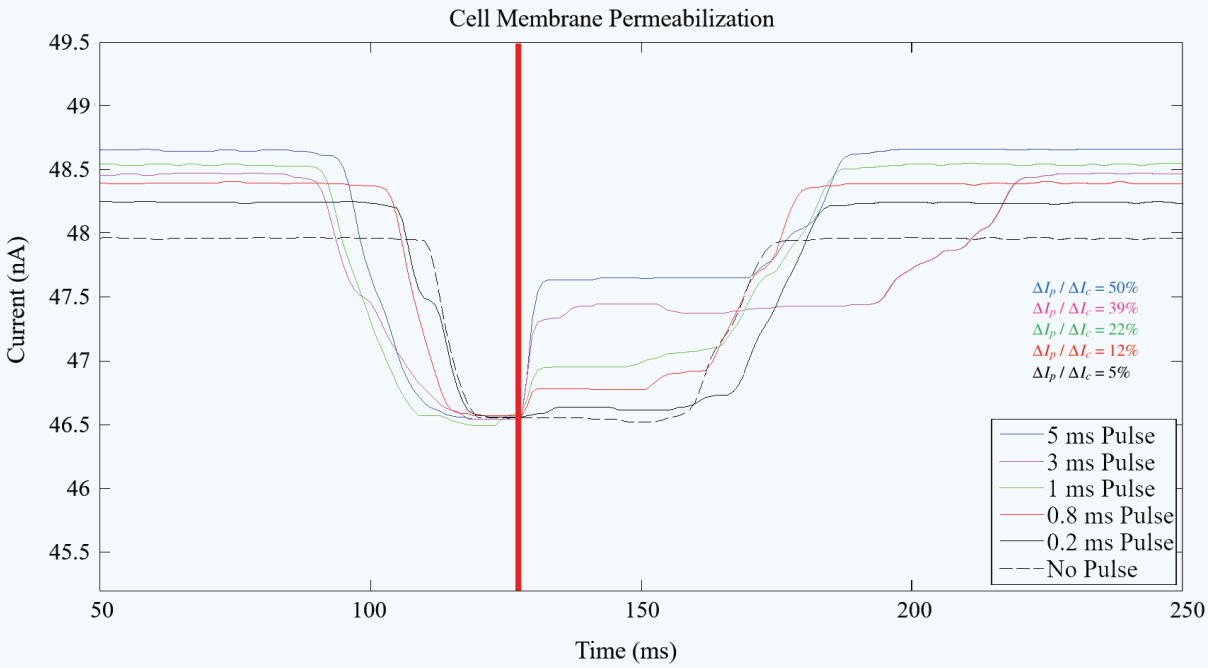

Figure 3 Electrical measurements of single cells that underwent electroporation treatment at 1.0 kV/cm electric field strength for 5.0 ms (blue trace), 3.0 ms (purple trace), 1.0 ms (green trace), 0.8 ms (red trace), 0.2 ms (black trace), compared with a single cell without electroporation treatment (dotted back trace). Cell membrane permeabilization, ΔI_p is normalized by its corresponding cell current displacement, ΔI_c and expressed according to their color-code.

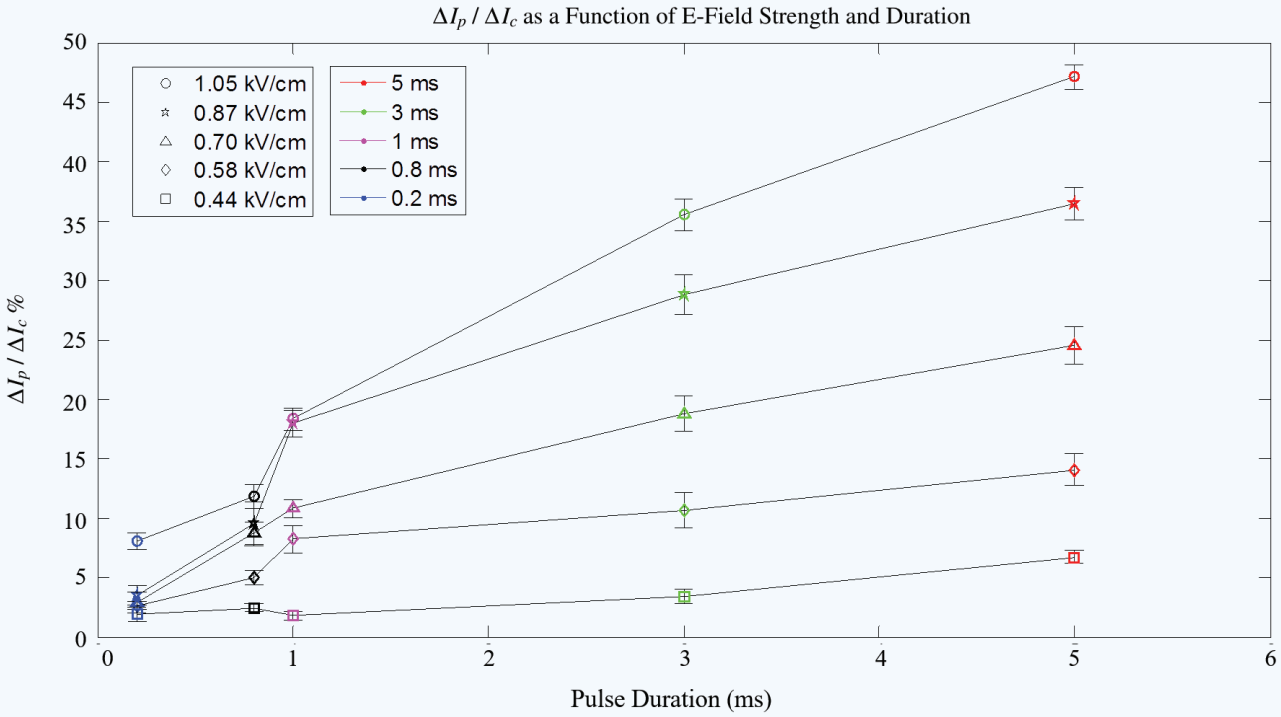

Figure 4 Normalized cell membrane permeabilization $\Delta I_p/\Delta I_c$ for single cells that underwent electroporation treatment with varying electric field strengths (0.44 – 1.05 kV/cm) and pulse duration (0.2 – 5.0 ms). $\Delta I_p/\Delta I_c$ represents the degree of cell membrane permeabilization for the corresponding pulse parameters. Electric fields are coded with symbols, whereas pulse durations are coded with color. 100 cells were averaged for each experimental condition.

normalized by the total cell-current displacement (ΔI_c) and expressed as a percentage increase from the detected cell-current baseline. When plotted as a function of pulse duration, a strong dependency was found between the normalized permeabilization current ($\Delta I_p/\Delta I_c$) and the pulse duration, for a given electric field strength. A strong dependence on electric field magnitude was also observed when different strengths were applied for the same pulse duration. For electric fields ranging from 0.58 to 1.05 kV/cm, a rapid transition in the permeabilization signal occurring when the pulse duration reaches and exceeds 1.0 ms was observed, with the largest change occurring when the field was 0.87 kV/cm and above. This electrical threshold for creating large, sustainable pores necessary for the intracellular delivery of therapeutic agents is consistent with numerous other observations during electroporation[10,30–35]. Since the system allows for continuous-flow and dynamic measurements of current, at least 100 cells were measured for each pulse condition, amounting to an analysis of over 2,500 individual cells. The impedance response due to the occurrence of multiple cells flowing through the electroporation zone simultaneously was omitted from the analysis, as the result is not indicative of single cell membrane permeabilization.

Permeabilization validation — propidium iodide fluorescence tracking

Cell membrane permeabilization was also verified optically by recording changes in fluorescence intensity that occur upon binding of propidium iodide (PI) to intercellular nucleic acids. An optical camera was synchronized with the lock-in amplifier sensor to capture a sequence of images within the electroporation zone of the pulsed cell immediately following each pulse application. These images were then evaluated for fluorescence intensity on an individual cell basis. **Figure 5** plots the fluorescence intensity of PI in a cell along with representative images of the cells as a function of both electric field strength and pulse duration. Since electroporation is an inherently polar phenomena, only the membrane surface at the cell poles (perpendicular to the applied electric field) becomes permeabilized once the transmembrane potential threshold is reached[30]. This transmembrane potential is further modulated by the natural membrane resting potential. Thus, the cell membrane closest to the positive electrode becomes hyperpolarized, resulting in a larger pore density compared to the side closest to the negative electrode. Further, since PI is positively charged, its delivery into the cell is enhanced by electrophoresis leading to the asymmetric delivery of propidium iodide into the hyperpolarized side of the cell. Larger pulse strengths and durations lead to greater cell membrane permeabilization, which in turn permit more PI entry through the porated cell membrane to bind with the nucleic acids in the cytoplasmic space, resulting in elevated fluorescence intensity.

A higher pulsing threshold is needed to produce optically distinguishable fluorescence intensities compared to the electrical measurements. This could be due to the greater sensitivity of the electrical system or that an electrical pulse that is sufficient for porating the cell membrane to change the electrical impedance may not be sufficient for delivery of PI. Optically, pulse durations longer than 1.0 ms were required to reliably correlate the degree of cell membrane permeabilization to the electrical parameters. For instance, in **Fig. 5**, a significant jump in fluorescence intensity can be identified after the 0.8 ms pulse duration for applied fields of 0.87 kV/cm and above, consistent with the electrical measurements of the permeabilization signal. This relationship is further verified by plotting the electrical-permeabilization signal ($\Delta I_p/\Delta I_c$) versus fluorescence intensity for all pulse strengths and durations (**Supplementary Fig. 3**). These data show a direct correlation between the amount of PI delivery and degree of membrane permeabilization, both of which are proportional to the electric-pulse parameters.

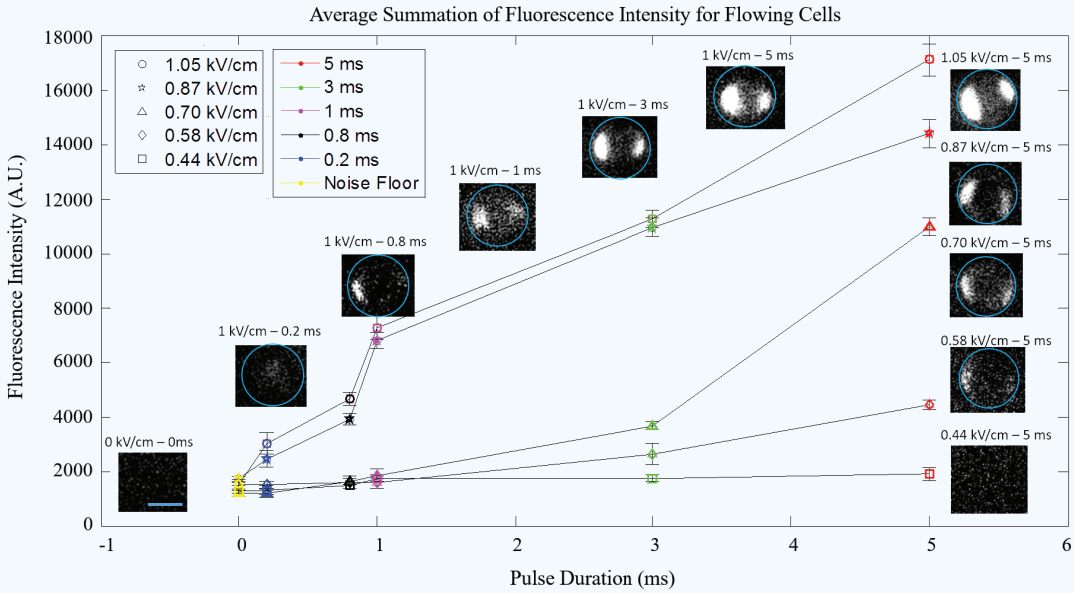

Figure 5 Optical measurement of propidium iodide fluorescence intensity in single cells after prescribed electroporation treatments with varying electric fields (0.44 – 1.05 kV/cm) and pulse duration (0.2 – 5.0 ms). Representative images of individual cells that underwent 1.05 kV/cm with varying pulse duration are plotted along the top curve; cells that underwent 5.0 ms pulse duration with varying electric field strength are shown on the right. 100 cells were averaged for each experimental condition. Scale bar in inset (0 kV/cm – 0 ms) represents a 10 µm length.

Cell viability study

The viability of single cells undergoing a prescribed electroporation treatment was also correlated with the electroporation-pulse parameters through 7AAD staining. Cells were recovered 20 minutes after being exposed to the electroporation pulse so that viable cells had time for membrane resealing. Histograms of 7AAD fluorescence intensity within cells exposed to 0.70, 0.87 and 1.05 kV/cm electric field strengths are shown in **Fig. 6a–c**. Within each histogram, the distribution of cells treated with three different pulse durations (0.5, 1.0, and 5.0 ms) are compared with live cells perfused through the microchannel but receiving no pulse treatment (black curve on left) and dead cells with "leaky" membranes (purple curve on right). The data were fitted

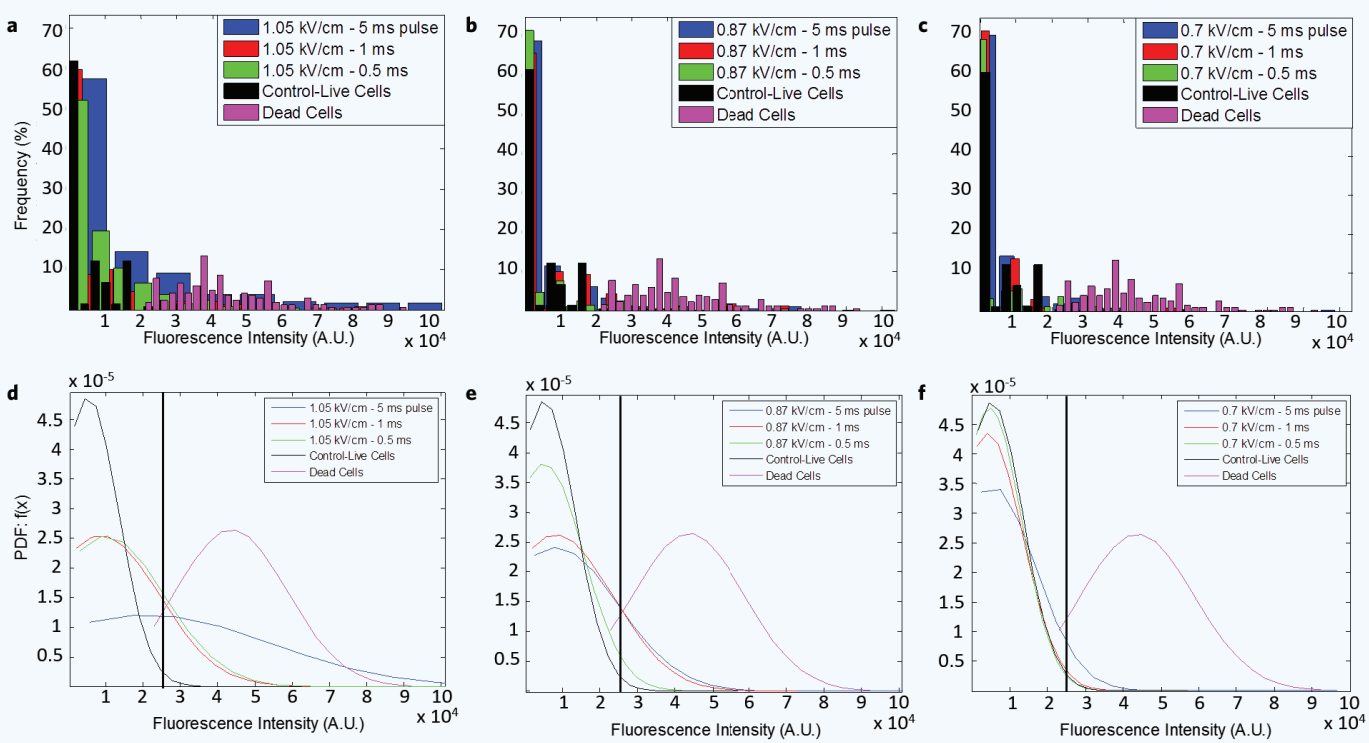

Figure 6 Histograms of cell populations treated with electroporation pulse at (**a**) 1.05 kV/cm (**b**) 0.87 kV/cm (**c**) 0.7 kV/cm from 0.5 to 5.0 ms pulse duration and (**d–f**) their respective normal curve fitting of the cell population histogram. Black vertical line in (**d–f**) marks the 95% confidence lower bound from the mean of the dead cell population fluorescence intensity. 200 cells were collected and analyzed for each experimental condition.

Table 1 Averaged 7AAD fluorescence intensity and cell viability percentage for different pulsing conditions.

Sample (n = 200/case)	7AAD intensity (a.u.)	Viability (%)
Live control	$5.2 \times 10^3 \pm 7.1 \times 10^2$	95.4
Dead control	$4.3 \times 10^4 \pm 1.2 \times 10^2$	—
Field strength 0.7 kV/cm		
0.5 ms	$4.7 \times 10^3 \pm 5.9 \times 10^2$	92.3
1.0 ms	$4.3 \times 10^3 \pm 9.5 \times 10^2$	86.1
5.0 ms	$5.3 \times 10^3 \pm 8.3 \times 10^2$	90.8
Field strength 0.87 kV/cm		
0.5 ms	$5.1 \times 10^3 \pm 7.7 \times 10^2$	92.3
1.0 ms	$8.2 \times 10^3 \pm 1.2 \times 10^3$	86.1
5.0 ms	$8.1 \times 10^3 \pm 9.5 \times 10^2$	86.6
Field strength 1.05 kV/cm		
0.5 ms	$1.04 \times 10^4 \pm 1.1 \times 10^3$	83.3
1.0 ms	$8.7 \times 10^3 \pm 1.0 \times 10^3$	85.1
5.0 ms	$2.1 \times 10^4 \pm 2.1 \times 10^3$	67.1

* The live cell control were cells that received zero pulse treatment, and the corresponding viability is representative of the intrinsic cell death occurring during experiments. Dead control were dead cells stained with 7AAD and retained an intact membrane.

with normal distributions to more clearly observe population shifts as the electrical parameters vary. A viability threshold (black vertical line in **Fig. 6d–f**) was determined for each of the cell populations by calculating the 95% confidence lower bound of the mean fluorescence intensity for the dead-cell population. Average 7AAD fluorescence intensity and the corresponding viability values for cells from each of the electroporation pulse conditions are listed in **Table 1**. The overall cell viability decreases monotonically with both increasing the electric field strength and pulse duration.

We found that cell viability was greater than 83% for all cases except the combination of the highest electric field strength (1.05 kV/cm) and pulse duration (5 ms), which caused the greatest shift towards the distribution of the dead cells, and the calculated viability dropped to 67.1%. This is expected since the strong electroporation treatment was more likely to irreversibly damage the cell membrane, hindering resealing. Decreasing the pulse strength (i.e. blue curves in **Fig. 6d–f**) or duration (i.e. blue and red curves in **Fig. 6d**) reduces the magnitude of the shift. All cells that underwent electroporation treatment at 0.7 or 0.87 kV/cm retained a comparable fluorescence to that of control live cells with calculated viability of 86% or higher, indicating complete resealing of the cell membrane within 20 minutes post-permeabilization. Therefore, the stronger pulsing condition (1.05 kV/cm) was more likely to cause irreversible cell membrane damage leading to cell death, whereas cells treated with moderate conditions (0.7 and 0.87 kV/cm) likely recovered, showing a higher population viability. Combining these results with the membrane impedance response, it is worth noting that a field strength of 0.87 kV/cm at a 1 ms duration results in a significant increase in membrane permeabilization, while preserving cell viability when compared to live cells. Such a regime of electroporation is of great interest when performing intracellular drug delivery studies.

Conclusion

We demonstrate the effectiveness of a continuous-flow based microelectroporation system that automatically detects and electroporates single cells with high accuracy and monitors the cell membranes electrical response. The electroporation system was validated both optically for intracellular molecular delivery and via a short-term viability assessment. This electroporation system demonstrated strong correlation of the degree of single cell membrane permeabilization to the applied electric fields in a continuous-flow environment, while permitting the collection and downstream processing of the treated cells. Cell membrane resealing has also been electrically observed in the course of our investigation. We are currently investigating its dynamic behavior and developing reliable means to control and enhance cell viability across various cell types, while improving the throughput of the system. Potential methods to increase the throughput of our system include: increasing cell density, device parallelization, or increasing the total number of electroporation zones, and increasing the operation speed of the automation software, allowing for higher flow rates in the device. Validating our device with multiple cell types will demonstrate the robustness of our system and the overall feasibility for using such a device in a biological setting. Such controllable electroporation of individual cells carries the promise to maximize cell viability across different cell types, providing an improved approach to the conventional empirical approach.

MATERIALS AND METHODS

Device fabrication

The device consists of a pair of planar electrodes on a glass substrate and a polydimethylsiloxane (PDMS) microchannel fabricated via soft lithography[14]. The silicon master mold with the device feature was fabricated using standard photolithographic procedures. The device main channel is 1 mm long, 150 μm wide, and 10 μm deep, incorporating a constriction with a dimension of 250 μm (L) × 25 μm (W) × 10 μm (D). Briefly, a 10 : 1 mixture of PDMS polymer and hardening agent was poured onto the mold to create a negative replica and allowed to cure at 65°C overnight. Holes were punched in the PDMS to create access to the inlet channel (0.5 mm in diameter) and to the outlet reservoir (1.5 mm in diameter). Titanium/Platinum (Ti/Pt) planar electrodes were fabricated via a metal "lift-off" process. Traces for the electrodes were patterned lithographically on glass substrates, and recesses were etched with 10 : 1 buffered hydrofluoric acid for 1 minute to a depth of ~ 2000 Å. The metals were deposited via physical vapor deposition (KJL PVD75, Kurt J. Lesker Co.) followed by dissolution of the photoresist in acetone leaving behind the electrode traces. The resultant Ti/Pt electrodes were 50 μm in width, with a center-to-center spacing of 300 μm. This distance allowed for sufficient cell transit time for electrical and optical analysis without compromising SNR quality. The surfaces of the PDMS and the glass substrate with patterned electrodes were treated under oxygen plasma at 100 W power, 250 sccm O_2 at 700 mTorr for 60 s (PX-250, March Instruments). The activated substrates were aligned using a stereo-microscope (SZ61 Binocular Stereo Zoom, Olympus) and irreversibly bonded. Copper wires were bonded to the planar electrode pads via conductive epoxy.

Experimental operation

Prior to each experiment, the microchannel was pre-treated with a 10% bovine serum albumin (BSA) solution at room temperature for one hour to prevent unwanted cell adhesion to the channel surfaces. The microchannel was then drained, and excess BSA solution was removed from the outlet reservoir and replaced with 10 μL of Dulbecco's modified Eagle's medium (DMEM) media. A precision microfluidic syringe pump (PicoPlus, Harvard Apparatus) was used to perfuse the cells at a flow rate of 0.1 μL/min, resulting in an average cell transit time of 250 ms across the microchannel constriction. Once a stable flow of single cells was established, the electroporation system was initiated upon user command. Five electric fields (0.44, 0.58, 0.70, 0.87, or 1.05 kV/cm, as measured at the cell) were investigated at five pulse durations each (0.2, 0.8, 1.0, 3.0, or 5.0 ms) to impose different degrees of cell membrane permeabilization.

Cell culture and harvest

NIH 3T3 mouse fibroblasts were cultured in DMEM supplemented with 10% v/v fetal bovine serum, 1% v/v penicillin–streptomycin, and 1% l-glutamine (Sigma-Aldrich, St. Louis, MO). Cells were cultured to 70% confluency before being harvested for experiments. The harvested cells were suspended at a concentration of 3 million cells per mL in an iso-osmotic electroporation buffer consisting of 250 mM sucrose, 10 mM HEPES, and 0.4 mM of M_gCl_2 salt to provide a conductivity of 100 μS/cm[9–11,14].

Cell assays

Two cell assays were carried out to validate the electroporation system. During the first assay, propidium iodide (PI) (P3566, Life Technologies), a cell membrane impermeant dye which fluoresces upon binding to cytosolic nucleic acids, was added to the electroporation buffer at 100 μM final concentration to optically signal membrane permeabilization. The electrical signal from a lock-in amplifier (HF2LI Lock-in Amplifier, Zurich Instruments) and the fluorescence intensity of PI delivery were recorded for each individual cell. In the second assay, single cells underwent the same electroporation treatments without PI addition. Following each prescribed pulse treatment, approximately 2000 cells were collected over 20 minutes from the outlet reservoir for viability assessment. The collected cells were washed in 1× PBS buffer via centrifugation at 2000 RPM for 2 minutes, then incubated with 2 μM of 7-Aminoactinomycin D (7AAD) (7AAD, ThermoFisher Scientific) on ice for 20 minutes to allow cell viability staining. The cells were then washed again in 1× PBS buffer prior to be imaged under a fluorescence microscope. A semi-automated cell scanning and processing algorithm written in MATLAB (MATLAB R2012b, Mathworks) was used to process the fluorescence intensity of the collected cells. Details regarding the assays, image acquisition, and processing have been described in our previous publication[14].

Cell impedance-based monitoring and electroporation

The lock-in amplifier was used to dynamically extract the signal and apply the electroporation pulse. A custom-built LabVIEW control algorithm was loaded onto the lock-in amplifier's embedded system for real-time processing. As shown in **Fig. 1c**, one device electrode was connected with the lock-in amplifier's waveform generator output via Lead I to deliver a sensing excitation signal of 1 V_{p-p}, while the other electrode was connected to a low-noise current preamplifier input (HF2CA Current Preamplifier, Zurich Instruments) via Lead II prior to passing the signal to the lock-in amplifier sensor. A frequency of 1.224 kHz was chosen to provide both optimal cell detection via the derivative-based peak-detection algorithm and the most sensitive cell membrane permeabilization detection with the highest SNR. When a cell is detected within the electroporation zone, an electroporation pulse is instantly delivered by a function generator (33220A Waveform Generator, Agilent) through Lead I to the monitoring oscilloscope via Lead III. The pulse was programmed in the function generator and fed to a high-voltage amplifier (Model 2350, TEGAM) to supply electric field pulses ranging from 0.44 to 1.05 kV/cm with a duration between 0.2 and 5.0 ms. A CMOS switch (DF419DJ+ Analog Switch, Maxim Integrated) synchronized with the function generator was added in series with the lock-in amplifier's preamplifier input to prevent measurement artifacts from the electroporation pulse[36]. The pulse trigger signal was also split to the external trigger input of a microscope mounted CMOS camera (PowerView 1.4MP, TSI) to simultaneously capture images of PI entry into cells following each pulse.

ACKNOWLEDGEMENTS

The authors would like to acknowledge financial support by the National Science Foundation (NSF CBET 0967598, DBI IDBR 1353918).

REFERENCES

1. Di Carlo, D. & Lee, L.P. Cell analysis for quantitative biology. *Anal. Chem.* **78**, 7918–7925 (2006).
2. Horan, P. & Wheeless, L. Quantitative single cell analysis and sorting. *Science* **198**, 149–157 (1977).
3. Wang, D. & Bodovitz, S. Single cell analysis: The new frontier in 'omics'. *Trends Biotechnol.* **28**, 281–290 (2010).
4. Cadossi, R., Ronchetti, M. & Cadossi, M. Locally enhanced chemotherapy by electroporation: Clinical experiences and perspective of use of electrochemotherapy. *Future Oncol.* **10**, 877–890 (2014).
5. Gehl, J. Electroporation: Theory and methods, perspectives for drug delivery, gene therapy and research. *Acta Physiol. Scand.* **177**, 437–447 (2003).
6. Woods, N. *et al.* Lentiviral vector transduction of NOD/SCID repopulating cells results in multiple vector integrations per transduced cell: Risk of insertional mutagenesis. *Blood* **101**, 1284–1289 (2003).
7. Kim, T.K. & Eberwine, J.H. Mammalian cell transfection: The present and the future. *Anal. Bioanal. Chem.* **397**, 3173–3178 (2010).
8. Bolhassani, A., Khavari, A. & Orafa, Z. Electroporation — Advantages and drawbacks for delivery of drug, gene and vaccine. In *Application of Nanotechnology in Drug Delivery*. (ed.) Sezer, A.D. (InTech, Rijeka, Croatia - EU, 2014).
9. Sadik, M.M., Li, J., Shan, J.W., Shreiber, D. I. & Lin, H. Quantification of propidium iodide delivery using millisecond electric pulses: Experiments. *Biochim. Biophys. Acta Biomembr.* **1828**, 1322–1328 (2013).
10. Sadik, M.M. *et al.* Scaling relationship and optimization of double-pulse electroporation. *Biophys. J.* **106**, 801–812 (2014).
11. Demiryurek, Y. *et al.* Transport, resealing, and re-poration dynamics of two-pulse electroporation-mediated molecular delivery. *Biochim. Biophys. Acta Biomembr.* **1848**, 1706–1714 (2015).
12. Li, J., Tan, W., Yu, M. & Lin, H. The effect of extracellular conductivity on electroporation-mediated molecular delivery. *Biochim. Biophys. Acta* **1828**, 461–470 (2013).
13. Yu, M., Tan, W. & Lin, H. A stochastic model for DNA translocation through an electropore. *Biochim. Biophys. Acta* **1818**, 2494–2501 (2012).
14. Zheng, M., Shan, J.W., Lin, H., Shreiber, D.I. & Zahn, J.D. Hydrodynamically controlled cell rotation in an electroporation microchip to circumferentially deliver molecules into single cells. *Microfluid. Nanofluid.* **20**, 16 (2016).
15. Li, J. & Lin, H. The current-voltage relation for electropores with conductivity gradients. *Biomicrofluidics* **4**, 13206 (2010).
16. Li, J. & Lin, H. Numerical simulation of molecular uptake via electroporation. *Bioelectrochemistry* **82**, 10–21 (2011).
17. Ryttsén, F. *et al.* Characterization of single-cell electroporation by using patch-clamp and fluorescence microscopy. *Biophys. J.* **79**, 1993–2001 (2000).
18. Huang, Y. & Rubinsky, B. Microfabricated electroporation chip for single cell membrane permeabilization. *Sens. Actuat. A Phys.* **89**, 242–249 (2001).
19. Khine, M., Lau, A., Ionescu-Zanetti, C., Seo, J. & Lee, L.P. A single cell electroporation chip. *Lab Chip* **5**, 38–43 (2005).
20. Khine, M., Ionescu-Zanetti, C., Blatz, A., Wang, L.-P. & Lee, L.P. Single-cell electroporation arrays with real-time monitoring and feedback control. *Lab Chip* **7**, 457–462 (2007).
21. Guo, X. & Zhu, R. Controllable in-situ cell electroporation with cell positioning and impedance monitoring using micro electrode array. *Sci. Rep.* **6**, 31392 (2016). doi:10.1038/srep31392.
22. Bürgel, S.C., Escobedo, C., Haandbaek, N. & Hierlemann, A. On-chip electroporation and impedance spectroscopy of single-cells. *Sens. Actuat. B Chem.* **210**, 82–90 (2015).
23. Lu, H., Schmidt, M.A. & Jensen, K.F. A microfluidic electroporation device for cell lysis. *Lab Chip* **5**, 23–29 (2005).
24. Wang, H.-Y. & Lu, C. High-throughput and real-time study of single cell electroporation using microfluidics: Effects of medium osmolarity. *Biotechnol. Bioeng.* **95**, 1116–1125 (2006).
25. Zhao, D. *et al.* A flow-through cell electroporation device for rapidly and efficiently transfecting massive amounts of cells *in vitro* and *ex vivo*. *Sci. Rep.* **6**, 18469 (2016).
26. Sun, T. & Morgan, H. Single-cell microfluidic impedance cytometry: A review. *Microfluid. Nanofluid.* **8**, 423–443 (2010).
27. Saleh, O.A. & Sohn, L.L. Quantitative sensing of nanoscale colloids using a microchip Coulter counter. *Rev. Sci. Instrum.* **72**, 4449 (2001).
28. Carbonaro, A. & Sohn, L.L. A resistive-pulse sensor chip for multianalyte immunoassays. *Lab Chip* **5**, 1155–1160 (2005).
29. Morgan, H., Sun, T., Holmes, D., Gawad, S. & Green, N.G. Single cell dielectric spectroscopy. *J. Phys. D Appl. Phys.* **40**, 61–70 (2007).
30. Gabriel, B. & Teissié, J. Time courses of mammalian cell electropermeabilization observed by millisecond imaging of membrane property changes during the pulse. *Biophys. J.* **76**, 2158–2165 (1999).
31. Smith, K.C., Neu, J.C. & Krassowska, W. Model of creation and evolution of stable electropores for DNA delivery. *Biophys. J.* **86**, 2813–2826 (2004).
32. Puc, M., Kotnik, T., Mir, L.M. & Miklavcic, D. Quantitative model of small molecules uptake after *in vitro* cell electropermeabilization. *Bioelectrochemistry* **60**, 1–10 (2003).

33. Beebe, S.J., Fox, P.M., Rec, L.J., Willis, E.L.K. & Schoenbach, K.H. Nanosecond, high-intensity pulsed electric fields induce apoptosis in human cells. *FASEB J.* **17**, 1493–1495 (2003).
34. Teissié, J., Escoffre, J.M., Rols, M.P. & Golzio, M. Time dependence of electric field effects on cell membranes. A review for a critical selection of pulse duration for therapeutical applications. *Radiol. Oncol.* **42**, 196–206 (2008).
35. Rols, M.P. & Teissié, J. Electropermeabilization of mammalian cells to macromolecules: Control by pulse duration. *Biophys. J.* **75**, 1415–1423 (1998).
36. Whittington, R.H., Giovangrandi, L. & Kovacs, G.T.A. A closed-loop electrical stimulation system for cardiac cell cultures. *IEEE Trans. Biomed. Eng.* **52**, 1261–1270 (2005).
37. Sun, T., Gawad, S.,. Green, N. & Morgan, H. Dielectric spectroscopy of single cells: Time domain analysis using Maxwell's mixture equation. *J. Phys. D-Appl. Phys.* **40**, 1–8 (2007).
38. Gentet, L.J., Stuart, G.J. & Clements, J.D. Direct measurement of specific membrane capacitance in neurons. *Biophys. J.* **79**, 314–320 (2000).

SUPPLEMENTARY INFORMATION

S1. Single cell impedance modeling before and after electroporation

The degree of cell impedance change as a result of electroporation-mediated membrane permeabilization can be assessed numerically using a cell/electrolyte circuit model. The resultant overall impedance equation for describing a membrane permeabilized cell including double layer effect is shown in Equation (S.1). $|Z|$ is the impedance magnitude of the single cell, ω is the angular frequency, and the formula for calculating the values of the individual electrical components, except for R_{mem}, can be found in previous work by Morgan and colleagues[37]. R_{mem} is based on the resistance of a typical patch of membrane R_M = 10000 Ω/cm^2[38], and assuming a spherical cell with radius r can be calculated as follows: $R_{mem} = \frac{R_M}{4\pi r^2}$. Electro-permeabilized cell membrane resistance $R_{porated\_mem}$ is conservatively approximated based on our previously published numerical model[13], assuming only 0.1% of the cell membrane is porated. $G_{mem} = 0.001\sigma_m(\frac{\pi r^2}{2d})$ where d is the membrane thickness of 5 nm and σ_m is the buffer conductivity at 100 μS/cm.

$$|Z| = \frac{1}{j\omega C_{DL}} + \frac{\left(R_m\left(1+R_i\left(j\omega C_{mem}+\frac{1}{R_{mem}}\right)\right)\right)}{\left(R_m\left(j\omega C_{mem}+\frac{1}{R_{mem}}\right)\right)+\left(1+R_i\left(j\omega C_{mem}+\frac{1}{R_{mem}}\right)\right)(1+j\omega R_m C_m)} \quad \text{(S.1)}$$

The impedance magnitude for an untreated cell is plotted as the black curve in **Supplementary Fig. 1a** and overlapped with the electroporated cell plotted in red. Change in impedance $\Delta|Z|$ as a result of varying R_{mem} from an intact (high R_{mem}) to permeabilized cell membrane state (low R_{mem}) falls in a frequency region between 1 and 10 kHz. The corresponding experimental data is shown in **Supplementary Fig. 1b**. A frequency sweep (100 Hz to 100 kHz) performed on an individual cell suspended in 100 μS/cm buffer before and after electroporation demonstrates a comparable impedance change in the frequency range predicted by the model.

To determine factors influencing $\Delta|Z|$ following electroporation, we systematically varied the cell volume fraction and extracellular buffer conductivity at different sweeping frequencies. The calculated result is shown as a contour map in **Supplementary Fig. 2**. We determined that the largest $\Delta|Z|$ following electroporation is dictated by both cell volume fraction and buffer conductivity at a lower frequency spectrum. This map provided a set of initial parameters to implement the permeabilization detection system. By using a micro-constriction channel to provide a cell volume-fraction of 5% and extracellular buffer conductivity at 100 μS/cm, a parameter which we previously reported to enhance electrophoretic transport of molecules into cell[9], the greatest change in cell membrane permeabilization following electroporation can be found using frequency ranges from 1 to 10 kHz.

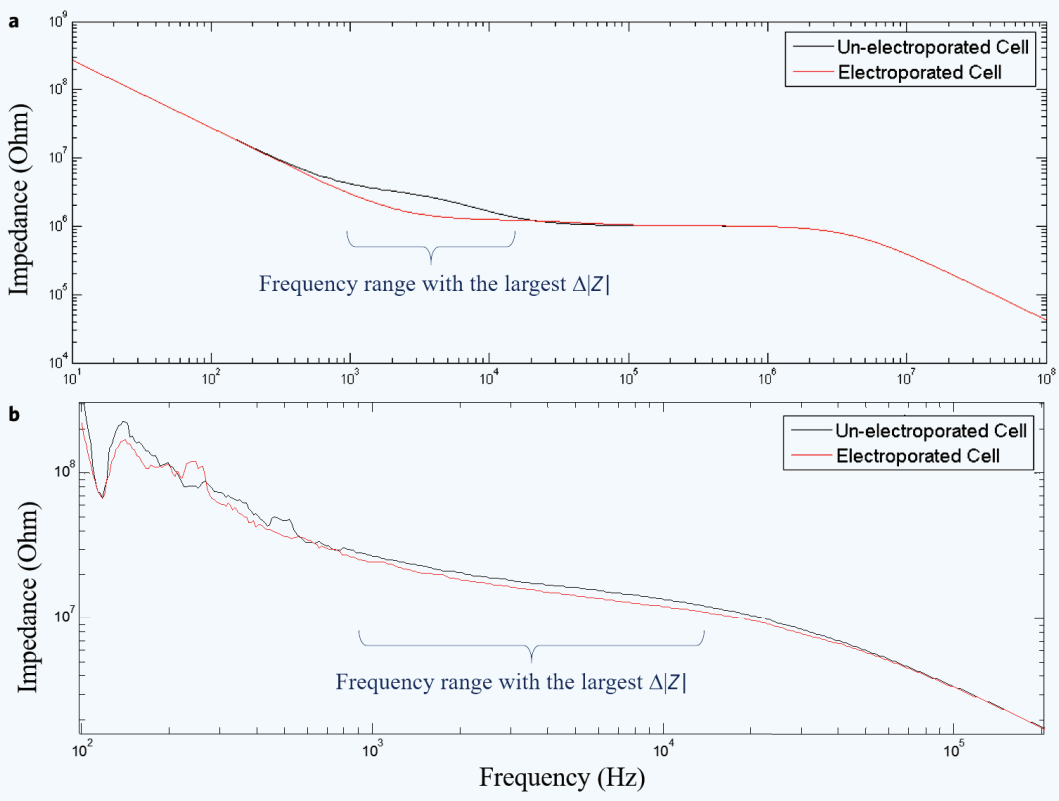

Supplementary Figure 1 (**a**) Simulated cell impedance as a function of frequency for an untreated (black curve) and treated (red curve) cell. Region of significant change in impedance $\Delta|Z|$ is shown from 1 to 10 kHz. (**b**) Experimentally measured change in cell impedance under the same conditions and parameters as that of the simulation.

S2. Intracellular molecular delivery based on cell membrane permeabilization

A direct relationship can be drawn between the cell membrane permeabilization and intracellular PI delivery. By combining the electrical and optical data onto one plot, such a link can be established to reveal

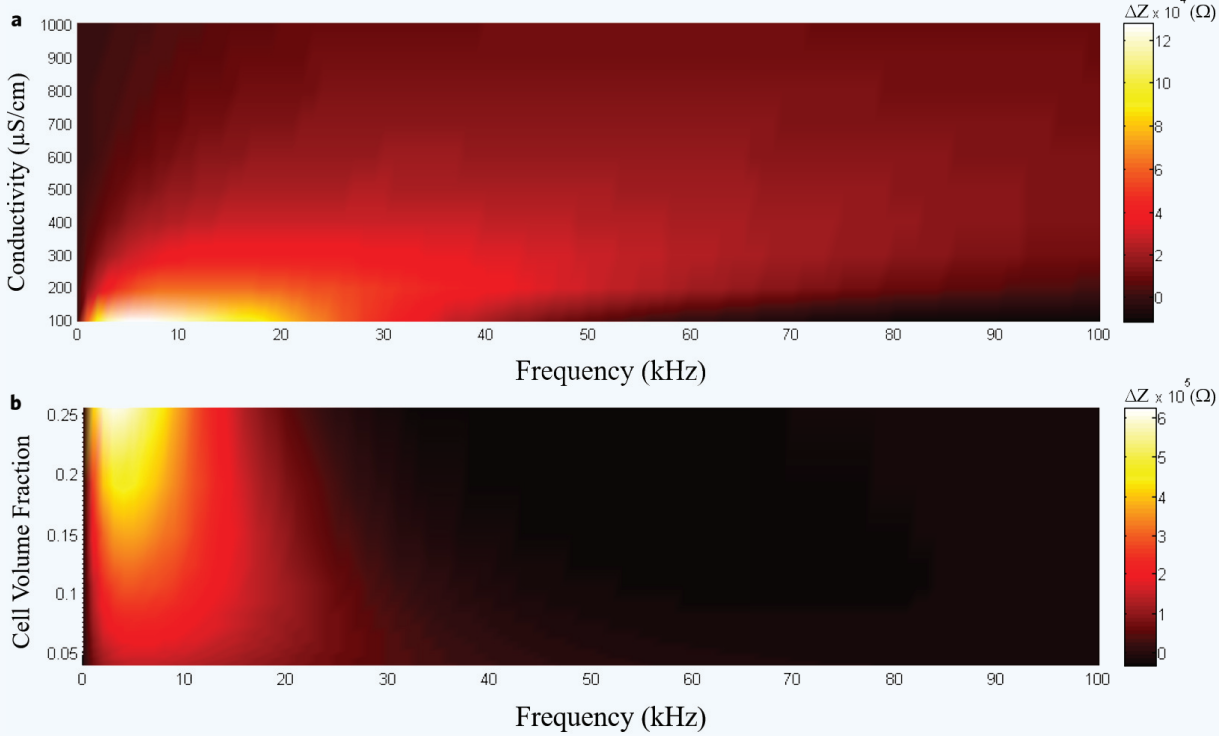

Supplementary Figure 2 Contour map displaying the calculated change in cell impedance Δ|Z| from a non-electroporated state to an electroporated state. Represented by color intensity, Δ|Z| is plotted as a function of frequency on the x-axis for (**a**) different extracellular buffer conductivities and (**b**) different cell volume fractions on the y-axis.

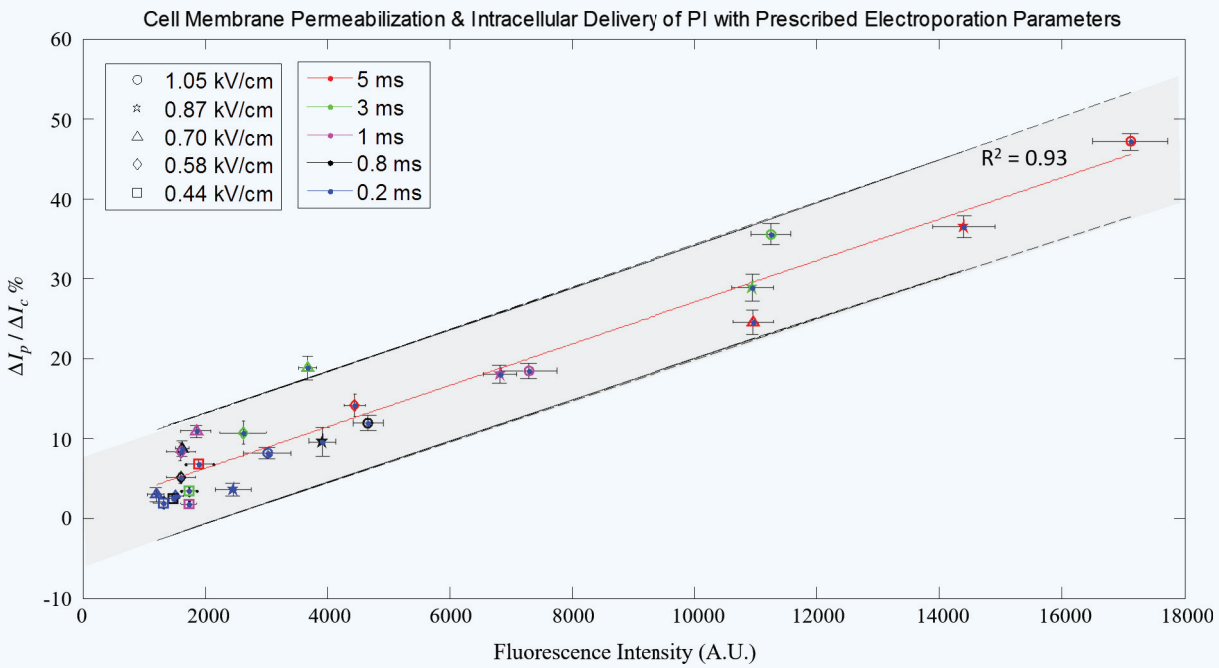

Supplementary Figure 3 Electrically-measured cell membrane permeabilization magnitudes ($\Delta I_p/\Delta I_c$) plotted as a function of PI fluorescence intensity in single cells following electroporation treatment with varying pulse strengths and duration. A linear curve fit applied to the ensemble data shows a positive correlation between the electrical and optical characterization of the cell membrane permeabilization with a shaded region indicating ± 1σ intervals.

the interdependent relationship between the two. **Supplementary Fig. 3** shows a scatter plot of points with the normalized membrane permeabilization magnitude along the *y*-axis and the corresponding fluorescence intensity for cells at that permeabilization state along the *x*-axis. The same symbols and colors used in **Fig. 6** and **Fig. 7** were used to differentiate the five groups of electric field strengths (symbols) and pulse duration (colors). Linear curve fitting was applied for each of the five electric field strengths and marked by labeled dashed lines. A linear and dependent relationship exists between the degree of membrane pore opening and the amount of PI delivered inside the cell. A large degree of poration is marked by a higher $\Delta I_p/\Delta I_c$ value, which corresponds to a greater extent of PI fluorescence intensity measured inside the treated cells.